CYGNSS Level 3 Merged Wind Speed Data Product for Storm Force and Surrounding Environmental Winds

April M. Warnock, Christopher S. Ruf, *Life Fellow, IEEE,* Anthony Russel, Mohammad M. Al-Khaldi, *Member, IEEE,* and Rajeswari Balasubramaniam, *Member, IEEE*

***Abstract*— A new wind speed product has been developed using bistatic radar data from NASA's Cyclone Global Navigation Satellite System (CYGNSS) mission. The product addresses shortcomings in two existing CYGNSS gridded wind speed products, the L3 Gridded Fully Developed Seas (FDS) Wind Speeds and the L3 Storm-Centric Gridded products, which individually are optimized for global, non-storm conditions and localized, high wind speed tropical cyclone conditions, respectively. In order to create a unified gridded wind speed product that captures both the storm force winds and the far-field environmental wind speeds, wind fields from the two products are merged onto a common grid. The algorithm produces global (+/- 40º latitude) windspeeds, averaged over a +/-6 hour window, and reported on a 0.1x0.1º grid. Gridded wind speeds are reported every 6 hours for each tropical cyclone when there are overpasses available during that time interval. The files are output on a storm-by-storm basis. Quadrant-dependent tropical cyclone 34-knot wind radii are estimated from the merged wind fields and included in the dataset. The performance of the merged wind speed product is validated against HWRF model output and SMAP tropical cyclone wind products, and the temporal and spatial sampling of the dataset is characterized. The dataset is found to exceed current temporal coverage capabilities compared to other existing tropical cyclone wind speed remote sensing instruments, although limitations on high wind speed retrievals and variable spatial coverage are notable and can be attributed to weaknesses of the underlying GNSS-R modality.**

***Index Terms*— Cyclone Global Navigation Satellite System (CYGNSS), Global Navigation Satellite System-Reflectometry (GNSS-R), tropical cyclone, ocean surface wind speed.**

I. INTRODUCTION

INCREASING tropical cyclone (TC) frequency and strength [1], combined with historically unprecedented populations in coastal regions [2] result in the need to better predict and provide guidance for these storms. For example, accurate and timely measurements of a TC's size (typically captured by measures of TC significant wind radii; distance from the TC center to a specific wind speed), structure (azimuthal variations in the wind radii), and intensity (typically measured by the maximum sustained windspeed, Vmax) are necessary for operational forecast models and to predict rapid intensification events that can be disastrous to coastal communities if timely evacuations are not carried out. While remote sensing instruments and in situ dropsondes deployed by airborne sensors (e.g., Hurricane Hunter aircraft) provide localized measurements of TC wind speeds [3], satellite remote sensing modalities of measuring TC winds provide the most practical means of achieving wide spatial coverage of TC wind fields. To this end, a number of TC wind speed products have been developed from satellite instruments. These satellite instruments fall primarily into the categories of scatterometers (e.g., ASCAT [4], HY-2C [5]), microwave radiometers (e.g., AMSR2 [6], SMAP [7], SMOS [8]), synthetic aperture radars (Sentinel-1 [9]), and, more recently, GNSS-R bistatic radars (CYGNSS [10,11], SPIRE [12]). Each of these remote sensing modalities have their limits, strengths, and weaknesses. For example, scatterometers are frequently used to measure TC wind radii, but the loss of signal sensitivity at high wind speeds can affect TC wind speed accuracy [13]. The signal from L-band microwave radiometers has the benefit of being largely impervious to precipitation, but the resolution can be too coarse to resolve fine-scale TC features [14,15]. SAR provides the highest spatial resolution of the aforementioned modalities (on the order of meters vs kilometers) and as such can identify fine-scale TC features [16], however, the availability of SAR imagery for operational TC applications is limited by low latency. While GNSS-R based TC wind retrievals are available at high revisit rates, the estimates contain greater uncertainty at high wind speeds [17]. A summary of strengths and weaknesses of a subset of currently operating satellite sensors with TC wind products is shown in Table I. A thorough review of TC wind speed products can be found in [18].

This work describes a new TC wind speed product based on data from the NASA Cyclone Global Navigation Satellite

This work was supported by the NASA Science Mission Directorate under Grant 80LARC21DA003 with the University of Michigan (UMich). (*Corresponding author: April Warnock.)*

April M. Warnock is with SRI International, Ann Arbor, MI, 48109 (email: april.warnock@sri.com).

Christopher S. Ruf, Rajeswari Balasubramaniam, and Anthony Russel are with the Department of Climate and Space Sciences and Engineering, University of Michigan, Ann Arbor, MI 48109 USA (e-mail: cruf@umich.edu; rajibala@umich.edu; russelan@umich.edu).

Mohammad M. Al-Khaldi is with the Department of Electrical and Computer Engineering, and the ElectroScience Laboratory, The Ohio State University, Columbus, OH 43210 USA (e-mail: al-khaldi.2@osu.edu).

System-Reflectometry (CYGNSS) mission. The CYGNSS constellation originally consisted of 8 microsatellites mounted with GNSS-R bistatic radar receivers, each capable of simultaneously tracking GPS specular reflections from four locations on the Earth's surface [21]. The tracks of a GNSS-R instrument are essentially pixel-wide swaths with an effective resolution of ~25km over the ocean. The CYGNSS constellation was launched into a low Earth orbit in December 2016 with the primary goal of measuring ocean surface wind speeds over the tropics and in particular, within the core of TCs. In November 2022, one satellite was lost, and the mission currently collects data from the remaining seven satellites, which are all in good health. Wind speeds are inferred from the CYGNSS data by using delay doppler maps (DDMs), to derive normalized bistatic radar cross-sections (NBRCS), from which wind speed is retrieved using a geophysical model function (GMF) that relates the NBRCS to surface wind speeds [17]. Through employment of a constellation of receivers operating at long wavelengths and the inclined orbit, the main strengths of the CYGNSS mission are frequent overpass rates, relatively low cost, and the ability to measure through rain and clouds.

TABLE I
COMPARISON OF EXISTING SATELLITE REMOTE SENSING INSTRUMENTS MEASURING TROPICAL CYCLONE WINDS

Mission	Type	Nominal resolution	Nominal revisit rate	Strengths	Weaknesses
SMOS	L-band radiometer	25 km	1-3 days	Impervious to precipitation	Relatively low spatial resolution [15,19]
				Wide swath width	
SMAP	L-band radiometer	38x49 km	2-3 days	Impervious to precipitation	Relatively low spatial resolution [14,15]
				Wide swath width	
AMSR2	Microwave radiometer	25 km	2 days	Additional channel for precipitation mitigation	No data available near landfall [18]
				Wide swath width	
Sentinel-1A/B	SAR	~30m	6 days	High resolution	Low revisit rate [20]
CYGNSS	GNSS-R	25 km	6-24 hours	Impervious to precipitation	Varying sparseness in temporal/spatial coverage [17]
				Relatively high revisit rate	Greater uncertainty at high wind speeds [17]
HY-2C	scatterometer	25 km	10 days	Wide swath	Sensitive to precipitation [13]
				Provides wind direction	Signal saturates at high wind speeds [13] Low revisit rate

A number of CYGNSS wind speed products have been produced with variations in the underlying algorithms that aim to optimize the retrieved wind speeds for specific conditions. E.g., the Level 3 Gridded Wind Speed product [22,23] contains two versions of estimated wind speeds; one for fully developed seas (FDS) conditions as would occur with low-moderate wind forcing, and a second for young seas limited fetch (YSLF) conditions such as occurs with TCs wind level forcing. These products are output on an hourly basis and as a result, each wind field contains significant gaps between tracks. To produce a data product that provides better spatial coverage of TCs, a second L3 data product was produced that collocates CYGNSS YSLF wind fields on a 0.2x0.2°grid over a 7.2x7.2° window centered on a given storm. This product, the Level 3 Storm-Centric Gridded (L3 SCG) wind speed product, collocates CYGNSS tracks over a longer window than the standard CYGNSS wind speed products, provides more comprehensive coverage of TC wind fields, and improves wind speed quality by employing both along-track and cross-track quality control (QC) [24]-[26]. Even with the longer averaging window, the L3 SCG product typically has coarser spatial coverage and greater variability compared to similar products provided by the SMAP and AMSR2 instruments [27], but the ability to measure storm winds several times a day allows for the possibility of capturing rapid intensification events that the latter sensors may miss.

This new TC wind speed product, the CYGNSS Level 3 Merged Storm (L3 MRG) wind speed data product [28], improves on the L3 SCG algorithm by merging the L3 SCG wind speeds with CYGNSS L3 FDS wind speeds far from the TC center. This approach produces 6-hourly gridded wind speeds for TCs over both the inner core region of the storm and across the wider surrounding area. The two products are merged over a transition zone between these two regions using a radially tapered averaging scheme over an annular region centered on the storm center and extending across the 34-knot wind radius. This merged wind speed product provides improved spatial coverage compared to the L3 SCG wind speed, and improved retrieval performance in the storm's inner core compared to the L3 FDS gridded wind speed. The inclusion of L3 FDS winds allows for global coverage in place of the limited 7.2x7.2° moving grid employed by the L3 SCG algorithm. A merged product, combining YSLF and FDS components in the appropriate regions near and far from a storm, also eliminates the need for end users of the wind product to decide for themselves which component is appropriate to use. In addition to the CYGNSS merged wind speeds, the L3 MRG algorithm produces quadrant-specific 34-knot wind radii estimates from the L3 MRG wind fields when sampling and storm structure allow.

II. Algorithm Description

A. Merged Wind Speed Algorithm Description

The L3 MRG algorithm produces data files for storms that are tracked by the National Hurricane Center (NHC) or the Joint Typhoon Warning Center (JTWC). The algorithm requires a priori knowledge of a TC's track to define the storm center at latitude φ_{BT} and longitude θ_{BT}, which are obtained by the Best Track files produced by these agencies. The storm tracks are provided by the NHC's Best Track files [29] for storms occurring in the Northern Atlantic and Eastern Pacific, and the JTWC for storms occurring in the Western North Pacific [30], North Indian Ocean [31], and over the Southern Hemisphere [32].

The L3 MRG wind speed algorithm transitions from 100% L3 SCG wind speeds to 100% L3 FDS wind speeds via a tapered weighted averaging scheme, over a radial distance defined by the storm's size. Because the L3 FDS wind speed product is defined on a 0.2x0.2° grid whereas the L3 SCG product uses a 0.1x0.1° grid, the L3 FDS product is resampled onto a 0.1x0.1° grid prior to the merging of the two windspeed products. The resampling subdivides each 0.2x0.2° grid cell into four 0.1x0.1° cells and assigns the same L3 FDS wind speed value to each cell.

The L3 MRG product produces wind fields on a 6-hourly cadence at 0000, 0600, 1200 and 1800 UTC whenever CYGNSS overpasses are available in a storm's vicinity for that 6-hourly interval. Otherwise, the 6-hourly interval is absent from the files. Since the L3 SCG product is generated at 6-hourly intervals, the L3 MRG algorithm uses the corresponding L3 SCG product directly. The L3 FDS product is generated at hourly intervals, therefore the L3 FDS wind field that is used in the merging algorithm is a composite of the L3 FDS products generated over a +/- 6-hour interval centered on each L3 MRG reporting time. L3 FDS samples are added to the composite grid beginning with the samples furthest in time from the center of the 12-hour time interval. If a sample is available at a closer time to the center of the 12-hour interval, it replaces any sample in the same grid cell from a more distant time relative to the reporting time. The measurement time offset (relative to the reporting time) of each FDS sample used is reported as ancillary information in the L3 MRG data product files. This composite approach provides a more fully populated L3 FDS grid for the L3 MRG algorithm and ensures that the reported winds are as close as possible to the center of the time interval.

The merging algorithm is defined with respect to three nested regions. The inner region corresponds to the inner core of the tropical cyclone. The outer region corresponds to distances far from the storm. The transition region is defined as the region between the inner and outer regions. The borders of the three regions are defined by the radial distance from the storm center, determined by the Best Track storm center location at the center time of the 12 hour time interval over which a particular L3 MRG product is generated. The radial distance from the storm center to the boundary of the inner core, R_{inner}, is given by

$$R_{inner} = \begin{Bmatrix} R25ms & if\ V_{max} \geq 25\ m/s \\ R_{max} - 50\ km & if\ V_{max} < 25\ m/s \end{Bmatrix}. \quad (1)$$

where *R25ms* is the minimum radial distance from the storm center outside of which all L3 SCG wind speeds are less than 25 m/s, V_{max} is the maximum L3 SCG wind speed, and R_{max} is the minimum radial distance from the storm center to the boundary of the 7.2x7.2° L3 SCG domain.

The radial distance R_{outer} is defined as the maximum distance from Vmax in the L3 SCG grid, less 50 km:

$$R_{outer} = \max(\mathrm{R}(\mathrm{u_{SCG}})) - 50\mathrm{km}. \quad (2)$$

The merging algorithm produces a merged wind speed, u_{MRG}, from the L3 SCG and FDS wind speeds, u_{SCG} and u_{FDS}, according to

$$u_{MRG} = \begin{Bmatrix} u_{SCG} & if\ r \leq R_{inner} \\ (1-a)u_{SCG} + au_{FDS} & if\ R_{inner} < r < R_{outer} \\ u_{FDS} & if\ r \geq R_{outer} \end{Bmatrix}, \quad (3)$$

where r is the radial distance from the storm center to the sample and $a = (r - R_{min})/(R_{max} - R_{min})$. Each L3 MRG wind speed is accompanied by its corresponding uncertainty value, σ_{MRG}, as defined by

$$\sigma_{MRG} = \begin{Bmatrix} \sigma_{SCG} & if\ r \leq R_{inner} \\ \sqrt{(1-a)^2\sigma_{SCG}^2 + a^2\sigma_{FDS}^2} & if\ R_{inner} < r < R_{outer} \\ \sigma_{FDS} & if\ r \geq R_{outer} \end{Bmatrix}, \quad (4)$$

where σ_{SCG} and σ_{FDS} are, respectively, the uncertainties of the SCG and FDS samples used.

An example of a merged wind field is shown in Fig. 1 for Hurricane Sam on Oct. 2, 2021, at reporting time 1200Z. The main figure shows the full wind field while the inset corresponding to the red box shows a region around the hurricane encompassing the storm and the transition region.

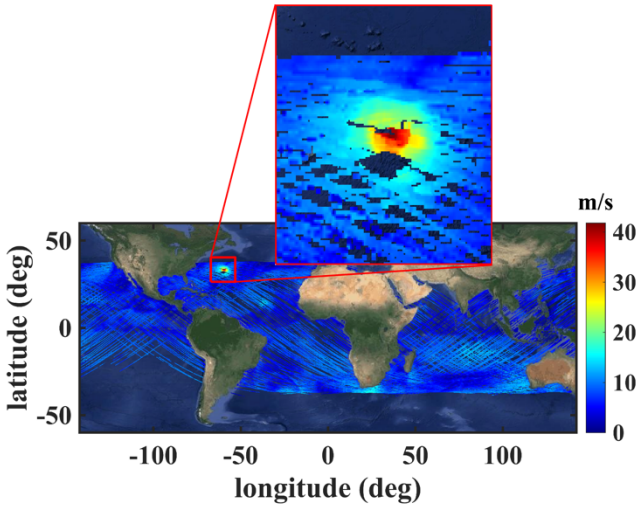

Fig. 1. Example L3 MRG wind field for Hurricane Sam on Oct. 2, 2021, 1200Z. The bottom figure shows the full merged wind field, while the inset zooms in on the region surrounding the storm.

B. CYGNSS 34-knot Wind Radii Algorithm

Quadrant-specific 34 kt (~17.5 m/s) wind radii (R34) are estimated directly from the CYGNSS L3 MRG wind fields and included in the L3 MRG data files. The inputs to the 34-knot radii algorithm are the L3 MRG wind field $u_{MRG}(\varphi, \theta)$ and estimated storm center at latitude φ_S and longitude θ_S. Note that φ_S and θ_S are not the Best Track storm center coordinates but rather the storm center estimated from the L3 MRG wind field, determined by locating the maximum wind speed in the inner region of the merged wind field.

An example of the R34 algorithm is shown here for the CYGNSS L3 MRG wind field depicted in Fig. 2 taken from the TC Calvinia (2020) data file. First, the wind field is projected onto an equivalent polar co-ordinate system $u_{MRG}(\Phi, d)$ as a function of azimuth (Φ) and radial distance (d) centered about an estimate of the storm's center using precomputed masks, examples of which are depicted in Fig. 3. The radial window extends 1000 km away from the storm center. The wind field is then azimuthally (Φ) integrated over the Northeast (NE), Southeast (SE), Southwest (SW) and Northwest (NW) quadrants using (5)-(8) respectively, collapsing the two-dimensional wind field into a radial profile:

$$u_{MRG}^{NE}(d) = \frac{1}{N_\Phi(d)} \sum_{\Phi=0}^{\Phi=\frac{\pi}{2}} u_{MRG}(\Phi, d) \quad (5)$$

$$u_{MRG}^{SE}(d) = \frac{1}{N_\Phi(d)} \sum_{\Phi=3\pi/2}^{\Phi=2\pi} u_{MRG}(\Phi, d) \quad (6)$$

$$u_{MRG}^{SW}(d) = \frac{1}{N_\Phi(d)} \sum_{\Phi=\pi}^{\Phi=\frac{3\pi}{2}} u_{MRG}(\Phi, d) \quad (7)$$

$$u_{MRG}^{NW}(d) = \frac{1}{N_\Phi(d)} \sum_{\Phi=\frac{\pi}{2}}^{\Phi=\pi} u_{MRG}(\Phi, d), \quad (8)$$

where N_Φ is the total number of samples at radial distance d in each quadrant. Examples of the resulting radial profiles for the wind field shown in Fig. 2 are depicted in Fig. 4.

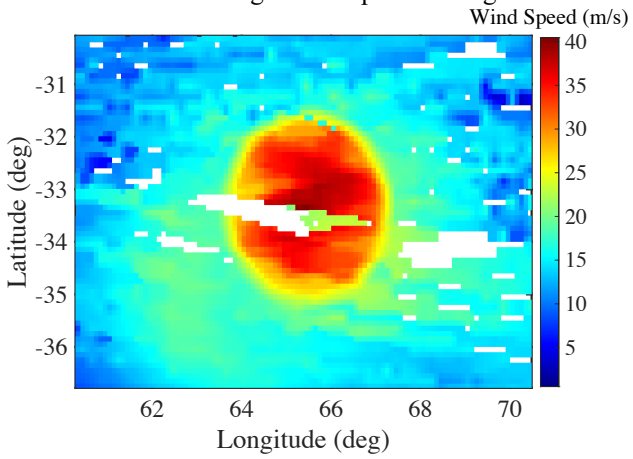

Fig. 2. Example CYGNSS L3 MRG wind field from TC Calvinia at 0600Z on Jan 1, 2020.

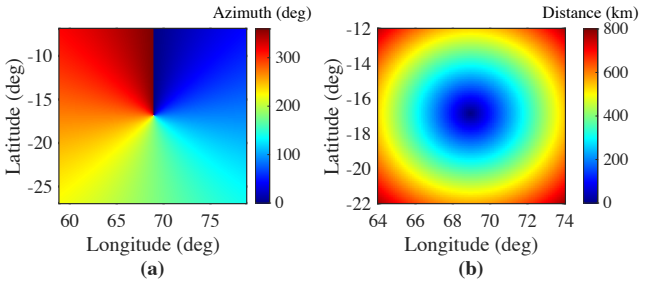

Fig. 3. Masks used for azimuthal integration of CYGNSS L3 MRG wind fields (a) azimuth relative to storm center; (b) radial distance relative to storm center.

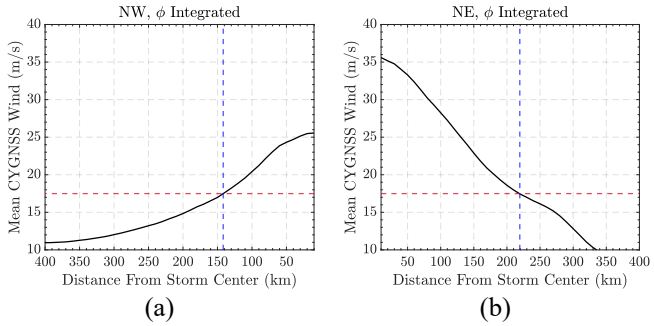

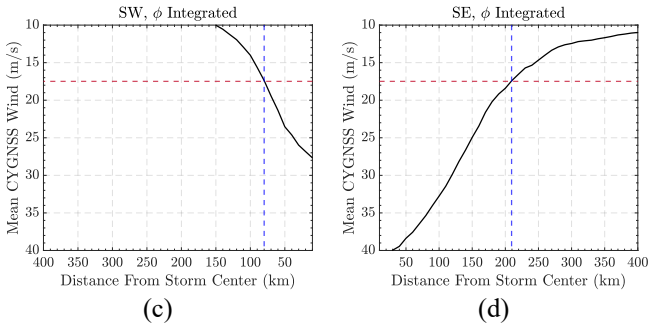

Fig. 4. Azimuthally integrated radial wind profiles. Red horizontal line indicates 34 kt (~17.5 m/s) point, blue vertical line indicates retrieved R34 value obtained using eqn. 9. (a) Northwest; (b) Northeast; (c) Southwest; (d) Southeast.

Subsequently, $R34^Q$ is estimated using (9) for every quadrant for which a u_{MRG}^{Q} value exceeding 34 kts is reported within a 500 km radial separation from the storm's center.

$$R34^Q = \underset{d*}{\operatorname{argmin}} \left| u_{MRG}^{Q}(d) - 34 \right| \quad (9)$$

By comparison of L3 MRG R34 retrievals to the Hurricane Weather Research and Forecast (HWRF) model [33] dataset over a multi-year period, we determined that retrieval performance is improved through the introduction of a quadrant specific debiasing term, summarized in Table II. The most likely cause of the bias is reduced sensitivity to higher wind speeds on the part of CYGNSS. This is consistent with the largest bias occurring in the NE quadrant where peak winds tend to be highest, and the smallest bias in the SW quadrant. The debiasing factors are applied to the radii obtained by (9) to calculate the final R34 estimates.

TABLE II
DEBIASING FACTORS FOR THE L3 MRG 34-KNOT WIND RADII

Quadrant	Debiasing Factor (km)
NE	71.19
SE	56.97
SW	37.19
NW	43.43

It is important to note that retrieval quality and related uncertainties of the R34 estimates are dependent on a variety of factors including level of storm development, specific observation geometries, range corrected gains and related variations across the subset of measurements used to form the L3 wind field, the adequacy of quadrant sampling (i.e. the percentage of a given quadrant with reported CYGNSS winds), and proximity to land. For example, the average difference between the Best Track storm centers and that used by the R34 algorithm (φ_s, θ_s) is 233 km, with a standard deviation of 144 km. These errors are likely caused by the sparse nature of the CYGNSS data, whereby an overpass directly over the storm's center during the reporting interval may not occur. Additionally, the saturation of the CYGNSS signal at high wind

speeds means that even when data is collected over the storm center, overall there will be a 'flattening' of the TC wind speeds that makes it more difficult to identify the true Vmax. The uncertainty in the location of the storm center based on the CYGNSS data has implications on the accuracy of the R34 estimates. The R34 estimation algorithm uses the CYGNSS-derived storm center to define the annulus over which the radial CYGNSS wind profiles are used to determine the R34 location in each quadrant, and as the result of a shifted storm center, the R34 algorithm may not capture the true radial wind speed profiles. In light of error sources such as this, quantification of R34 retrieval uncertainty as a function of these dependencies and further improvements to the algorithm are anticipated as part of future product releases.

III. PERFORMANCE CHARACTERIZATION AND VALIDATION

A. Coverage Statistics

1) Temporal Coverage: To determine the CYGNSS L3 MRG temporal coverage, we calculate statistics based on the percentage of 6-hourly increments over a storm's lifecycle that an L3 MRG wind field is reported. We define the lifecycle of a storm based on storm status time series reported in the Best Track files, where a storm's lifecycle is considered having begun when it meets the criteria of having well defined surface circulation, e.g., a status of low (LO) or tropical depression (TD). The storm's lifecycle is considered complete just prior to the time that the storm reaches and remains in either extratropical (EX), low (LO), or disturbance (DB) status, or if the Best Track record ends. Note that the L3 MRG files often contain wind fields corresponding to times outside of this definition of storm lifecycle since the Best Track files frequently contain data for times that extend outside this window. These wind fields are excluded from the temporal coverage analysis. Storms that never reach tropical storm level are also excluded, as well as storms that do not have status reported. With these exclusions the L3 MRG SDR v3.2 data record covers 360 named storms over 2019-2023. The temporal coverage over this dataset averages 57.5%, with a range 8-78%, and a standard deviation of 12%. A histogram of the temporal coverage over the 360 storms analyzed is shown in Fig. 5.

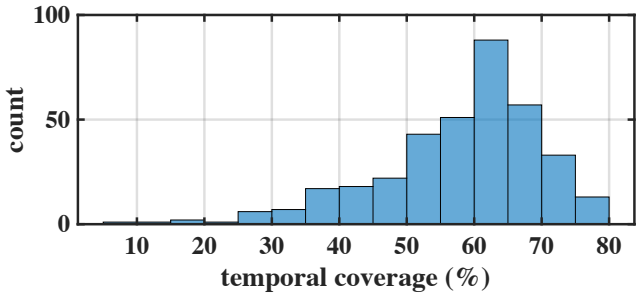

Fig. 5. Histogram of the number of 6-hourly increments that contain an L3 MRG wind field over a storm's lifecycle.

Examples of temporal coverage for individual storms are shown in Fig. 6, where the green dots in each panel indicate Best Track storm center locations and the red circles indicate an L3 MRG wind field is available for the time corresponding to that Best Track point. Fig. 6(a) shows an example of relatively low temporal coverage (12%) for Hurricane Erick (lifecycle: 7/27/2019 12Z – 8/04/2019 18Z), Fig. 6(b) shows an example of mid-range temporal coverage (46%) for Tropical Storm Pabuk (lifecycle: 12/30/2018 12Z – 01/06/2019 06Z), and Fig. 6(c) shows an example of high coverage (76%) for Hurricane Tammy (lifecycle: 10/11/2023 12Z – 10/26/2023 00Z).

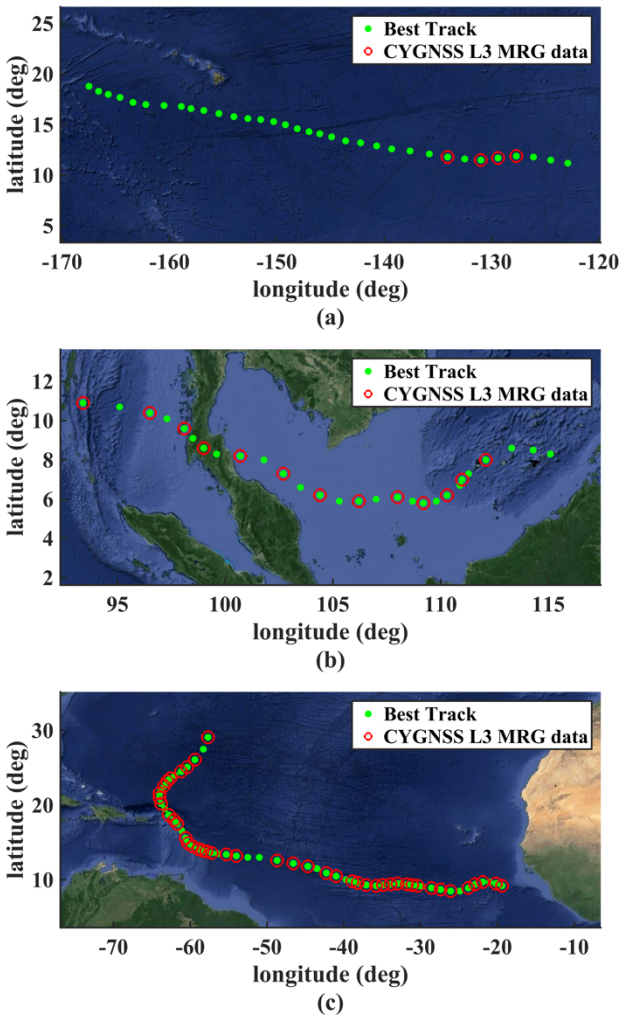

Fig. 6. Examples of low, medium, and high L3 MRG temporal coverage for Hurricane Erick (2019) at 12% coverage (a), Tropical Storm Pabuk (2018) at 46% coverage (b), and Hurricane Tammy (2023) at 76% coverage.

A detailed view of temporal coverage is shown in Fig. 7 for Hurricane Enrique (lifecycle: 6/25/2021 06Z – 6/30/2021 12Z) where the grid rows are the days covering Enrique's lifecycle, the columns are the 6-hourly reporting times, and the plots are L3 MRG wind fields in the vicinity of the storm. The temporal coverage for this storm is 59%, and the L3 MRG availability varies from 0-3 out of 4 reporting periods per day.

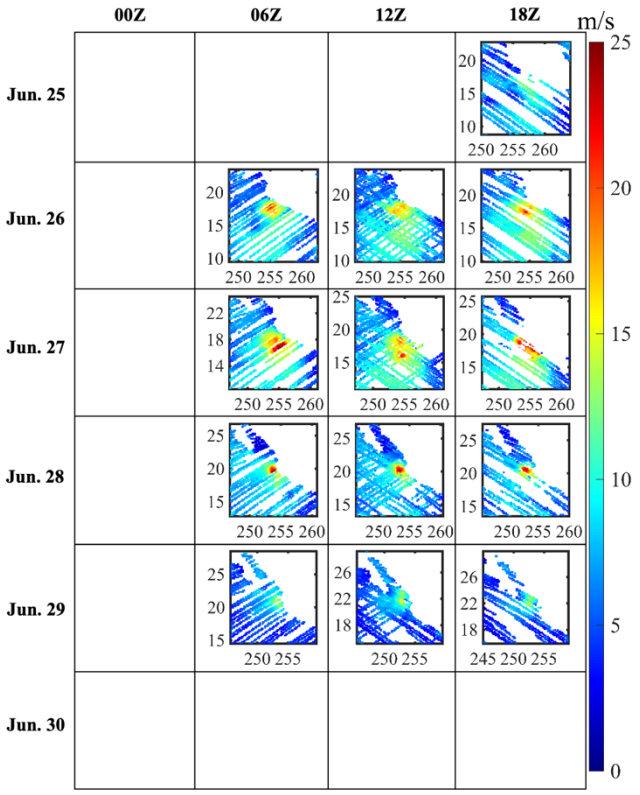

Fig. 7. Wind field coverage for Hurricane Enrique (2021). Storm lifecycle: 6/25/2021 06Z – 6/30/21 12Z. The CYGNSS L3 MRG coverage is 59%.

A second full lifecycle view is shown in Fig. 8 for a longer lasting storm, Typhoon Wutip, that by our definition has a lifecycle of 2/19/2019 00Z – 2/28/2019 06Z. The L3 MRG temporal coverage for Typhoon Wutip is 71%.

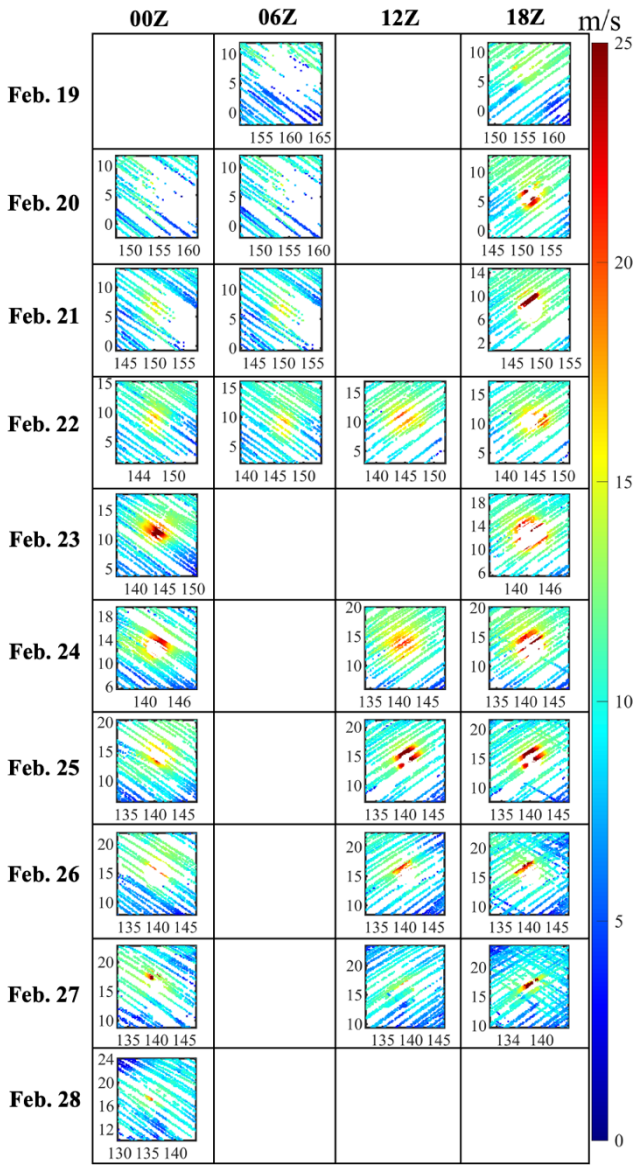

Fig. 8. Wind field coverage for Typhoon Wutip (2019). Lifecycle: 2/19/2019 00Z – 2/28/2019 06Z. The L3 MRG temporal coverage is 71%.

A breakdown of the number of daily overpasses over the 360 storm dataset is shown in Table III. Based on these statistics, the most likely number of overpasses (the mode) is 3 and the average number of overpasses is 2.1.

TABLE III
NUMBER OF OVERPASSES PER DAY OVER A 360 STORM DATASET

Number of overpasses per day	0	1	2	3	4
% of dataset	10.7	11.1	34.1	43.5	0.6

2) Spatial Coverage: To characterize the spatial coverage of the L3 MRG SDR v3.2 dataset with respect to storm winds, statistics are generated by calculating the fraction of the L3 MRG grid that contains wind speeds for two regions: (1) the region that extends from the CYGNSS estimated storm center at latitude φ_S and longitude θ_S to the Best Track reported R34 radii to quantify inner core coverage, and (2) the region that

extends from the Best Track reported R34 value to 2*R34, to quantify outer core coverage. For both regions, a single R34 value is determined by taking the maximum of the available quadrant-specific 34 knot radii reported in the Best Track files. Wind fields where R34 values are not reported are excluded from the analysis. This results in a total of 4893 wind fields that are analyzed for inner and outer core spatial coverage. Note that these wind fields include all the wind fields available in the L3 MRG files, including those that fall outside of our storm lifecycle definition bounds. The histograms in Fig. 9 summarize the fractional coverage distribution for the inner core (Fig. 9(a)) and outer core (Fig. 9(b)). The average inner and outer core coverages are 61.6% and 56.3%, with standard deviations of 21% and 19%, respectively.

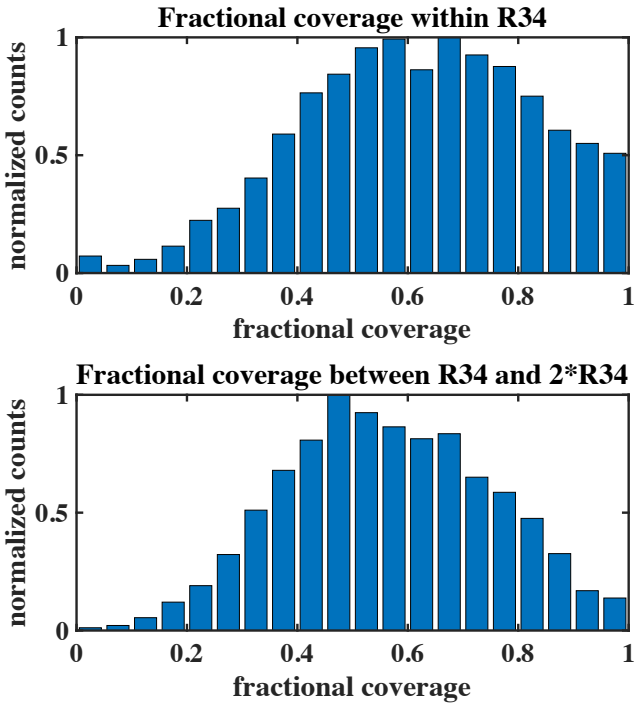

Fig. 9. Normalized histograms of the fractional inner core (a) and outer core (b) coverage over 4893 L3 MRG wind fields.

Examples of varying spatial coverage are shown for three storms in Fig. 10. Fig. 10(a) shows a wind field from Hurricane Otis, a relatively small storm. In this case the L3 MRG wind field largely excludes the inner core on the TC (15% coverage) but the outer core is fairly well-represented at 65% coverage. Fig. 10(b) shows a wind field from Hurricane Tammy. The L3 MRG wind field captures more of the inner core of the TC in this case, but the coverage still contains significant gaps. In Fig. 10(c), a well-sampled wind field for Hurricane Sam is shown, where the inner and outer core coverage are ~90%.

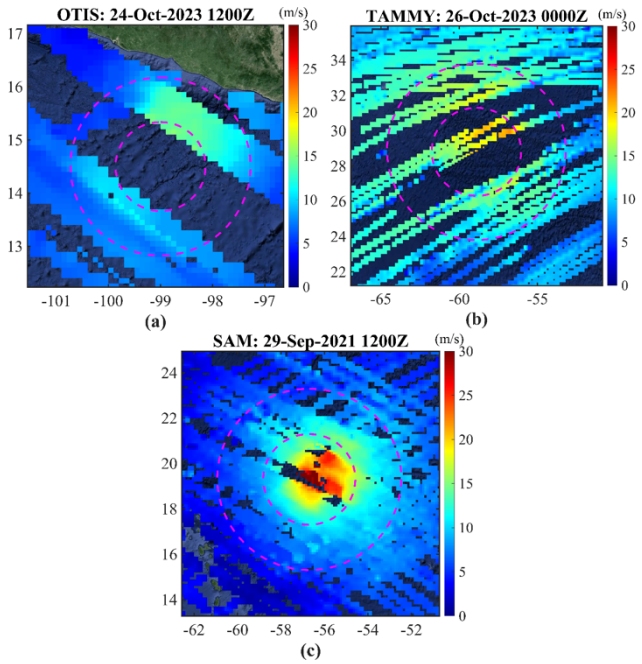

Fig. 10. Examples of varying spatial coverage for 3 hurricanes: (a) Otis, with inner and outer core spatial coverages of 15% and 65%, respectively; (b) Tammy, with inner and outer core spatial coverages of 30% and 51%, respectively; and (c) Sam, with inner and outer core spatial coverages of 89% and 91%, respectively. The magenta circles represent the Best Track 34-knot wind radii (inner circles) and the radii at double the Best Track 34-knot wind radii (outer circles).

B. Wind Field Comparisons to HWRF

For analysis of the CYGNSS L3 MRG wind speeds, measurements over major hurricanes from 2018-2022 of the L3 MRG SDR v3.2 dataset were used. Comparisons were conducted with respect to HWRF reanalysis winds and Soil Moisture Active Passive (SMAP) radiometer winds. HWRF is an operational model developed by the National Centers for Environmental Prediction (NCEP). HWRF provides 3 domains (one parent and 2 nested) and is based on the initial position of the storm and on the National Hurricane Center (NHC) forecast of the 72-hour storm position. The 2 nested domains move along the storm with a coverage of 24 deg x 24 deg and 7 deg x 7 deg for the middle and the inner nest respectively. For our purposes, we use the inner nest gridding that offers the finest resolution of about 0.015 deg (approx. 2 kms). The CYGNSS wind speed estimates are matched to the HWRF inner nest grid, which has a spacing of 2 kms. The HWRF winds are re-sampled to CYGNSS resolution and are co-located to CYGNSS wind estimates with a maximum temporal separation of 60 minutes and a maximum spatial separation of 0.25 deg latitude and longitude. Fig. 11 shows a log-density scatter plot of the matched-up CYGNSS and HWRF winds where the colorscale indicates the log of the density in units of samples per grid cell. The RMSD and bias between the CYGNSS and HWRF match ups for wind speeds less than 30 m/s are 5.75 and 3.28 m/s, respectively, and for wind speeds less than 40 m/s are 8.5 and 5.9 m/s, respectively.

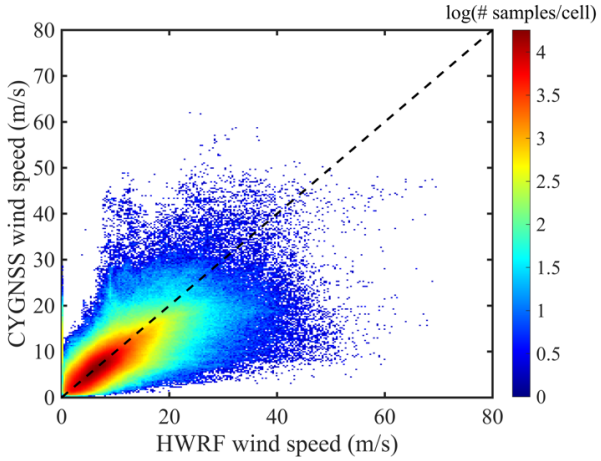

Fig. 11. Log-density scatter plot between CYGNSS L3 MRG and HWRF wind measurements in hurricanes. The RMSD and bias for wind speeds less than 30 m/s are 5.75 and 3.28 m/s, respectively, and for wind speeds less than 40 m/s are 8.5 and 5.9 m/s, respectively.

The CYGNSS L3 MRG winds are then filtered to only include samples where the quality flag is set to zero. As with the wind speed product itself, the quality filter is a merging of the filters used by the two wind speed products being merged. For samples within the R34 radius arising from the L3 SCG data product, the quality flag tests for consistency between wind speed measurements made by different satellites in the same grid cell. This filter is described in [24, 25]. For samples outside of the R34 radius arising from the L3 FDS data product, the quality flag as described in [22] leverages quality flags at earlier (Level 1 and 2) stages of data processing which test for nominal hardware status and limit checks on a variety of engineering parameters. Filtering the dataset to samples where the quality flag is set to zero results in a total dataset consisting of approximately 13.57 million observations in and around hurricanes. Fig. 12 shows the comparison of distribution of wind speeds between HWRF and CYGNSS. It can be observed that the HWRF wind speed distribution has a longer tail than CYGNSS, implying a possible saturation of CYGNSS measurements at about 50 m/s. Fig. 13 shows the performance of CYGNSS L3 MRG winds with respect to HWRF reference winds using RMSD and bias as the metrics. The bias here is defined as $(u_{HWRF} - u_{CYG})$. Below 5 m/s there is a negative bias indicating that CYGNSS overestimates compared to HWRF, and the bias gradually increases with wind speed indicating that CYGNSS begins to underestimate winds compared to HWRF with increase in wind speed. The RMSD is less than 10 m/s up to wind speeds of about 25 m/s, which is considered to be low-moderate range wind speeds and can become as high as 20 m/s at very high winds (~ 40 m/s). Above 40 m/s the CYGNSS measurements get saturated and the RMSD gets driven by bias alone and therefore is not reliable.

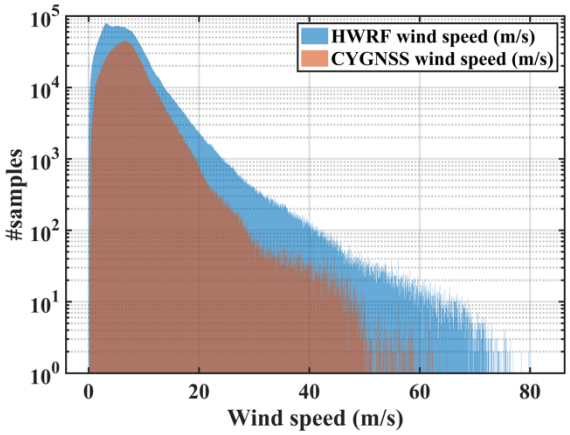

Fig. 12. Wind speed distribution in the CYGNSS-HWRF matchup dataset.

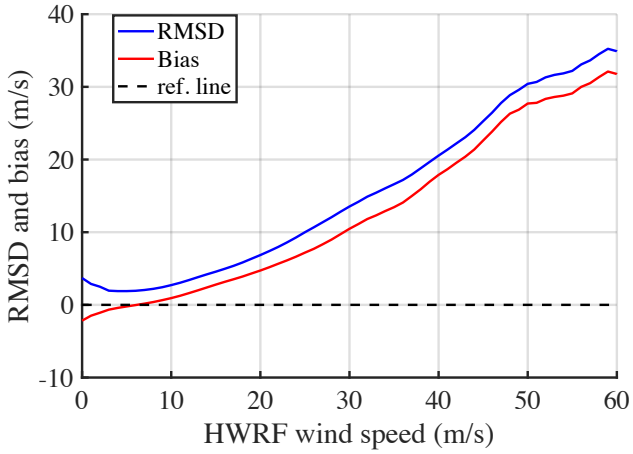

Fig. 13. RMSD and bias of CYGNSS L3 MRG winds compared to HWRF reference winds.

C. Wind Field Comparisons to SMAP

The above comparisons were repeated with winds from the SMAP radiometer as the reference. The SMAP satellite observatory consists of both an active radar and a passive radiometer sharing a common L-band feed horn. The passive L-band radiometer generates surface measurements at a resolution of 39x47 kms with a repeat cycle of approximately 8 days. The SMAP data product developed by Remote Sensing Solutions (RSS) [34] is used as a reference in this analysis. These data products are Level 3 daily gridded products with a grid spacing of 0.25 deg. The CYGNSS-SMAP matchup data is developed by co-locating CYGNSS and SMAP winds within a spatial separation of 0.25 latitude/longitude and 180 mins of temporal separation. This results in a total dataset of about 2.85 million samples. Fig. 14 shows a log-density scatter plot of the matched-up CYGNSS L3 MRG and SMAP winds, where the colorscale indicates the log of the density in units of samples per grid cell. The RMSD and bias between the CYGNSS and SMAP match ups for wind speeds less than less than 30 m/s are 6.92 and 5.17 m/s, respectively, and for wind speeds less than 40 m/s are 9.9 and 8.03 m/s, respectively. Fig. 15 shows the wind speed distribution in the dataset and Fig. 16 shows the RMSD and bias with respect to SMAP winds. A comparison of Figs. 12 and 15 indicates there is consistency in RMSD and bias

between the L3 MRG dataset and the two independent reference datasets.

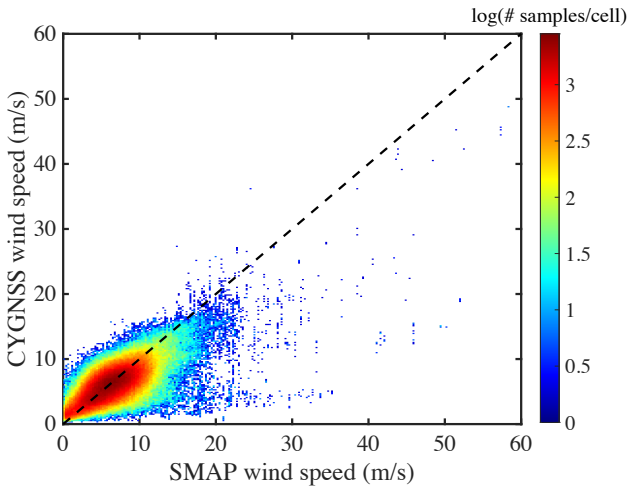

Fig. 14. Log-density scatter plot between CYGNSS L3 MRG and SMAP wind measurements in hurricanes. The RMSD and bias for wind speeds less than 30 m/s are 6.92 and 5.17 m/s, respectively, and for wind speeds less than 40 m/s are 9.9 and 8.03 m/s, respectively.

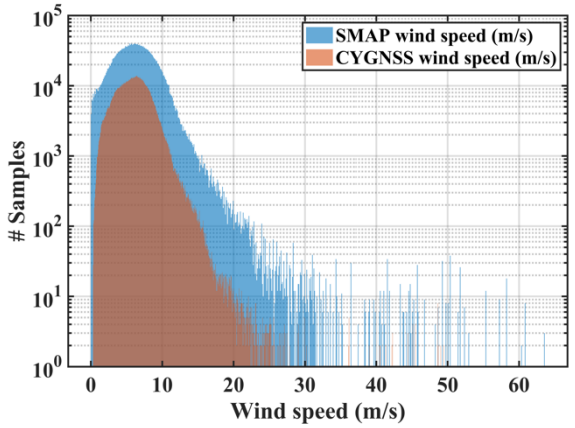

Fig. 15. Wind speed distribution in the CYGNSS-SMAP matchup dataset.

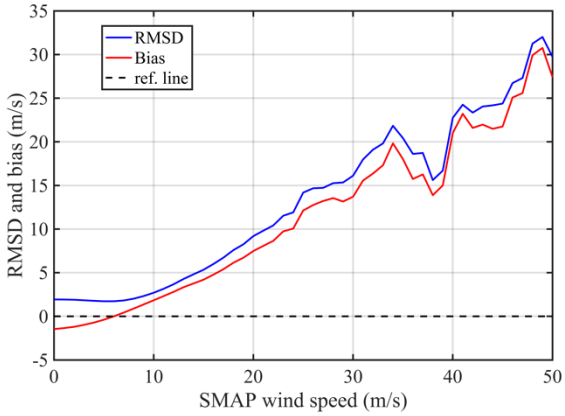

Fig. 16. RMSD and bias of CYGNSS L3 MRG winds compared to SMAP reference winds.

D. 34-knot Wind Radii Performance

1) Temporal coverage: Because the L3 MRG storm files may cover a period that extends beyond the closed-circulation stages of a storm, R34 values are not relevant to many of the L3 MRG wind fields. Therefore, to determine the temporal coverage of the L3 MRG R34 product, only wind fields with a Best Track reported status of Tropical Depression (TD), Tropical Storm (TS), or Hurricane (HU) are used in the analysis. Note that the HU category includes storms categorized in the Best Track files as Typhoons because of their occurrence in the Southern Hemisphere. Further, it can be expected that a storm's size and strength will impact the ability of the L3 MRG algorithm to return R34 value, so we break up the analysis to cover the categories of TD, TS, and HU individually. This process results in a total of 1222 TD wind fields, 2897 TS wind fields, and 1773 HU wind fields. The statistics for the temporal availability of R34 values of each of these categories is shown in Table IV. In general, it can be seen that there is a correlation between storm status and R34 availability, with the percentage of wind fields producing any R34 quadrant estimates greatest for the HU category (69%), and least for the TD category (11%). The number of quadrants that are retrieved is also correlated to storm status. Of the wind fields that generate at least one quadrant specific R34 estimate, only one quadrant is reported over 30% of these wind fields for the TD category, 17% for the TS category, and 9% for the HU category. This pattern holds for the percent of wind fields that return exactly 2 and 3 quadrant estimates in each category, with the HU category overall providing the greatest percentage of wind fields that return all four R34 quadrant retrievals (62%).

TABLE IV
PERCENT OF WIND FIELDS WHERE QUADRANT-SPECIFIC 34-KNOT WIND RADII ARE AVAILABLE

	TD	TS	HU
wind fields with no R34 values reported (%)	89	71	31
wind fields with any R34 values reported that report 1 quadrant (%)	30	17	9
wind fields with any R34 values reported that report 2 quadrants (%)	32	21	11
wind fields with any R34 values reported that report 3 quadrants (%)	23	24	18
wind fields with any R34 values reported that report 4 quadrants (%)	15	38	62

2) *Comparison to HWRF:* The accuracy of the CYGNSS L3 MRG 34-knot quadrant-specific wind radii are characterized by comparison to R34 values provided by HWRF. Fig. 17 compares HRWF R34 estimates to CYGNSS over 175 reference wind fields. The RMSD over all data points is 90.1 km, the bias is -1.2 km, and the unbiased RMSD (URMSD) is 80.8 km. While the retrievals span a wide range of R34s that include estimates as small as ~50 km and as large as ~450 km, the R value is 70.1%, indicating good correlation to the HWRF

34-knot wind radii.

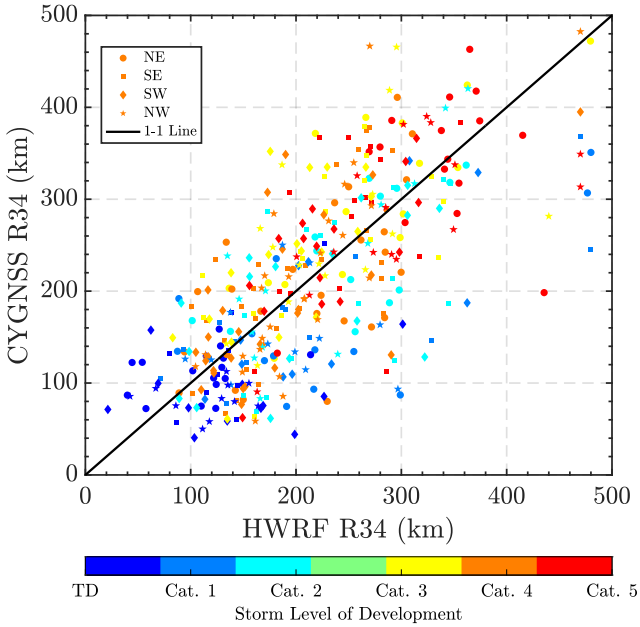

Fig. 17. Quadrant-specific 34-knot wind radii retrieval comparisons to HWRF using a CYGNSS data record spanning 175 reference HWRF wind fields, where the symbols signify the quadrant (circles = NE, squares = SE, diamonds = SW, and stars = NW), and the color designates the Best Track storm category from TD to Category 5 HU. Correlation estimated to be ~70%.

IV. Discussion

A primary motivation for development of the new L3 MRG data product is the desire to eliminate complications associated with having two distinct wind speed products – one in fully developed seas and the other in young seas with limited fetch. The origin of this distinction is the sensitivity of GNSS-R measurements not only to the smaller capillary waves which are directly forced by local surface winds, but also to longer swell waves. The balance between shorter and longer wave portions of the ocean surface roughness spectrum are in equilibrium in a fully developed sea but tend to be less so in organized cyclonic storms, where wind speed and direction can change significantly on much shorter time scales and fetch lengths. As a result, the same GNSS-R measurement can correspond to two different wind speeds, depending on whether the measurement is made in well developed or young seas. By merging the two products together across the transition zone from young to fully developed seas in the vicinity of the 34 knot wind radius, data users are provided with a single wind speed product that is applicable in both the inner core of storms and in the background environmental wind field through which the storm passes. In terms of data usage, the L3 MRG product is intended to support data assimilation schemes for the numerical weather prediction of storms, which require inputs for both the inner core and surrounding winds.

The flight segment architecture of the CYGNSS mission was designed to maximize the frequency of storm measurements. With its constellation of 8 satellites (now 7 as of November 2022) all operating at a shallow 35° orbit inclination, there are L3 MRG products generated in either 2 or 3 of the 6 hr intervals in a day for 78% of the days throughout a storm's lifecycle, with 1 6-hourly product generated for 11% of the days and no product generated the other 11% of the time. This high temporal sampling rate is to be compared to that provided by a traditional scatterometer or microwave radiometer wind sensor on a polar orbiting platform with a 2 or 3 day revisit time. For a 2 day revisit, a single 6-hourly observation of the storm is produced 50% of the time, no observation is produced 50% of the time, and multiple observations in a day are never produced. For a 3 day revisit, one 6-hourly observation is produced 33% of the time and no observation is produced 67% of the time.

The 6-hourly reporting interval of the L3 MRG product is chosen to be consistent with the standard initialization cadence used by operational hurricane numerical prediction models. The window of data collection (12 hr) is chosen to be twice as wide as the reporting interval (6 hr) in order to satisfy the Nyquist sampling criteria for time varying signals. Use of a 12 hr window precludes changes on time scales of less than 12 hrs from being resolved, and the L3 MRG wind fields are reported at twice the rate of the shortest resolvable changes. It should be noted that use of a 12 hr window results in some individual samples being used in two successive 6-hourly reports. This is a general feature of time averaged signals that are reported at or above the Nyquist rate.

The quality of CYGNSS measurements of ocean surface wind speed varies with the wind speed itself. The underlying cause is a decrease in the strength of the GPS signal scattered from the ocean surface in the forward (specular) direction as the surface roughness increases with increasing wind speed. In addition, the rate of change of the scattered signal strength with respect to wind speed also decreases as wind speed increases. These two dependencies are represented by the Geophysical Model Function (GMF) that maps wind speed to scattering cross section, and the slope of the GMF with respect to wind speed. The GMF and its development are described in detail in [17]. This general tendency will be true of all wind sensors using the GNSS-R remote sensing technique. A direct consequence of this behavior for the L3 MRG data product is an increase in the uncertainty of its wind speed estimates as the wind speed increases, and a significant loss of sensitivity above ~40 m/s. One possible mitigation strategy to recover the high wind sensitivity has been considered in [35] not for CYGNSS but for possible follow on missions. While the behavior of the GMF at high wind speeds is an intrinsic property of ocean surface scattering and not mission specific, the ability to accurately measure the weaker scattered signal at high wind speeds can be improved by increasing the signal-to-noise ratio of the measurements. A specific engineering approach to improving the measurement SNR is addressed in [35].

V. Summary

A new gridded wind speed product has been developed that merges two existing CYGNSS L3 gridded data products to produce unified wind fields that optimize the CYGNSS data both near and far from storm force winds. The merged data product requires ancillary Best Track storm latitudes and longitudes and produces files for all TCs that are tracked by the NHC and JTWC. When sampling is adequate, 34-knot wind

radii are estimated from the merged wind fields.

Analysis of the resulting L3 MRG SDR v3.2 dataset indicates that the product excels at providing high temporal coverage of TCs, with an average of 2.1 overpasses per day and an average of 57.5% temporal coverage over TC lifecycles. The spatial coverage of the L3 MRG wind fields near TCs is highly variable, with average inner and outer core coverages of 61.6% and 56.3% and standard deviations of 21% and 19%, respectively. Comparison to other sources of TC wind speed products (HWRF and Remote Sensing Solution's SMAP TC wind product) indicates a consistent bias towards lower wind speeds. This is consistent with observed behavior of GNSS-R derived wind speeds that demonstrate saturation at high wind speeds and greater uncertainty at storm-force winds.

The 34-knot wind radii produced from the L3 MRG wind fields correlate well with reference (HWRF) values, but the dataset has considerable scatter, likely due to the above-mentioned issues with accurately measuring higher wind speeds, locating the storm center in the CYGNSS L3 MRG wind fields, and the unreliable spatial coverage of the inner and outer cores of the storms. Future product releases will be aimed at improving the R34 algorithm performance and characterizing the uncertainty in the estimates. Overall, while there are notable caveats to the dataset, the improved coverage of storm-force winds provided by the L3 MRG dataset should provide an unprecedented source of TC wind speed data for assimilation and storm guidance applications.

ACKNOWLEDGMENT

The authors would like to thank Dr. Lisa Bucci at the National Hurricane Center for providing support for this manuscript.

REFERENCES

[1] Seneviratne, S.I., X. Zhang, M. Adnan, W. Badi, C. Dereczynski, A. Di Luca, S. Ghosh, I. Iskandar, J. Kossin, S. Lewis, F. Otto, I. Pinto, M. Satoh, S.M. Vicente-Serrano, M. Wehner, and B. Zhou, 2021: Weather and Climate Extreme Events in a Changing Climate. In Climate Change 2021: The Physical Science Basis. Contribution of Working Group I to the Sixth Assessment Report of the Intergovernmental Panel on Climate Change [Masson-Delmotte, V., P. Zhai, A. Pirani, S.L. Connors, C. Péan, S. Berger, N. Caud, Y. Chen, L. Goldfarb, M.I. Gomis, M. Huang, K. Leitzell, E. Lonnoy, J.B.R. Matthews, T.K. Maycock, T. Waterfield, O. Yelekçi, R. Yu, and B. Zhou (eds.)]. Cambridge University Press, Cambridge, United Kingdom and New York, NY, USA, pp. 1513–1766, doi:10.1017/9781009157896.013.

[2] Jan-Ludolf Merkens, Lena Reimann, Jochen Hinkel, Athanasios T. Vafeidis, Gridded population projections for the coastal zone under the Shared Socioeconomic Pathways, Global and Planetary Change, Volume 145, 2016, Pages 57-66, ISSN 0921-8181, https://doi.org/10.1016/j.gloplacha.2016.08.009.

[3] Collins, Jennifer, and Paul Flaherty. "The NOAA hurricane hunters: a historical and mission perspective." *The Florida Geographer* 45 (2014).

[4] Verspeek, Jeroen, et al. "Validation and calibration of ASCAT using CMOD5. n." *IEEE Transactions on Geoscience and Remote Sensing* 48.1 (2009): 386-395. 10.1109/TGRS.2009.2027896.

[5] Z. Wang et al., "Scatterometer Sea Surface Wind Product Validation for HY-2C," in IEEE Journal of Selected Topics in Applied Earth Observations and Remote Sensing, vol. 14, pp. 6156-6164, 2021, doi: 10.1109/JSTARS.2021.3087742.

[6] Imaoka, K., et al. "Instrument performance and calibration of AMSR-E and AMSR2." *International archives of the photogrammetry, remote sensing and spatial information science* 38.8 (2010): 13-18.

[7] Meissner, Thomas, Lucrezia Ricciardulli, and Frank J. Wentz. "Capability of the SMAP mission to measure ocean surface winds in storms." *Bulletin of the American Meteorological Society* 98.8 (2017): 1660-1677. [3] Kerr, Yann H., et al. "Soil moisture retrieval from space: The Soil Moisture and Ocean Salinity (SMOS) mission." *IEEE transactions on Geoscience and remote sensing* 39.8 (2001): 1729-1735. https://doi.org/10.1175/BAMS-D-16-0052.1

[8] Reul, N., Tenerelli, J., Chapron, B., Vandemark, D., Quilfen, Y., and Kerr, Y. (2012), SMOS satellite L-band radiometer: A new capability for ocean surface remote sensing in hurricanes, *J. Geophys. Res.*, 117, C02006, doi:10.1029/2011JC007474.

[9] Gao, Y.; Sun, J.; Zhang, J.; Guan, C. Extreme Wind Speeds Retrieval Using Sentinel-1 IW Mode SAR Data. *Remote Sens.* **2021**, *13*, 1867. https://doi.org/10.3390/rs13101867.

[10] Clarizia, M. P., and C. S. Ruf, 2016, "Wind Speed Retrieval Algorithm for the Cyclone Global Navigation Satellite System (CYGNSS) Mission," IEEE Trans Geosci. Remote Sens., 54(8), doi:10.1109/TGRS.2016.2541343.

[11] Rose, R., C. Ruf, D. Rose, M. Brummitt, A., Ridley, 2013, "The CYGNSS Flight Segment; A Major NASA Science Mission Enabled by Micro-Satellite Technology," Proc. 2013 IEEE Aerospace Conf., Big Sky, MT., 1-13, doi: 10.1109/AERO.2013.6497205.

[12] Philip Jales, Stephan Esterhuizen, Dallas Masters, Vu Nguyen, Oleguer Nogués Correig, Takayuki Yuasa, Jessica Cartwright, "The new Spire GNSS-R satellite missions and products," Proc. SPIE 11533, Image and Signal Processing for Remote Sensing XXVI, 1153316 (20 September 2020); https://doi.org/10.1117/12.2574127.

[13] Li, X.; Yang, J.; Wang, J.; Han, G. Evaluation and Calibration of Remotely Sensed High Winds from the HY-2B/C/D Scatterometer in Tropical Cyclones. Remote Sens. 2022, 14, 4654. https://doi.org/10.3390/rs1418465.

[14] Meissner, T.; Ricciardulli, L.; Manaster, A. Tropical Cyclone Wind Speeds from WindSat, AMSR and SMAP: Algorithm Development and Testing. Remote Sens. 2021, 13, 1641. https://doi.org/10.3390/rs13091641.

[15] Ricciardulli, L., Howell, B., Jackson, C.R., Hawkins, J., Courtney, J., Stoffelen, A., Langlade, S., Fogarty, C., Mouche, A., Blackwell, W. and Meissner, T., 2023. Remote Sensing and Analysis of Tropical Cyclones: Current and Emerging Satellite Sensors. Tropical Cyclone Research and Review.

[16] Horstmann, J., Wackerman, C., Falchetti, S., & Maresca, S. (2013). Tropical cyclone winds retrieved from synthetic aperture radar. Oceanography, 26(2), 46-57.

[17] Ruf, Christopher S., and Rajeswari Balasubramaniam. "Development of the CYGNSS geophysical model function for wind speed." IEEE Journal of Selected Topics in Applied Earth Observations and Remote Sensing 12.1 (2018): 66-77.

[18] John A. Knaff, Charles R. Sampson, Matthew E. Kucas, Christopher J. Slocum, Michael J. Brennan, Thomas Meissner, Lucrezia Ricciardulli, Alexis Mouche, Nicolas Reul, Mary Morris, Galina Chirokova, Philippe Caroff, Estimating tropical cyclone surface winds: Current status, emerging technologies, historical evolution, and a look to the future, Tropical Cyclone Research and Review, Volume 10, Issue 3, 2021, Pages 125-150, ISSN 2225-6032, https://doi.org/10.1016/j.tcrr.2021.09.002.

[19] Cotton, J., Francis, P., Heming, J., Forsythe, M., Reul, N. and Donlon, C. (2018), Assimilation of SMOS L-band wind speeds: impact on Met Office global NWP and tropical cyclone predictions. Q.J.R. Meteorol. Soc, 144: 614-629. https://doi-org.sri.idm.oclc.org/10.1002/qj.3237.

[20] Rucci, Alessio, et al. "Sentinel 1 SAR interferometry applications: The outlook for sub millimeter measurements." Remote Sensing of Environment 120 (2012): 156-163.

[21] Ruf, C. S., R. Atlas, P. S. Chang, *M. P. Clarizia*, J. L. Garrison, S. Gleason, S. J. Katzberg, Z. Jelenak, J. T. Johnson, S. J. Majumdar, A. O'Brien, D. J. Posselt, A. J. Ridley, R. J. Rose, V. U. Zavorotny," New Ocean Winds Satellite Mission to Probe Hurricanes and Tropical Convection," Bull. Amer. Meteor. Soc., doi:10.1175/BAMS-D-14-00218.1, 2016.

[22] Ruf, C., 2021, Level 3 Gridded Wind Speed. CYGNSS Algorithm Theoretical Basis Document. UM Doc. No. 148-0319, Rev 2, 13 Oct 2021.

[23] CYGNSS. 2022. CYGNSS Level 3 Climate Data Record Version 1.2. Ver. 1.2. PO.DAAC, CA, USA. Dataset accessed [YYYY-MM-DD] at https://doi.org/10.5067/CYGNS-L3C12

[24] Mayers, D., 2021, Level 3 Storm-Centric Gridded Wind Speed. CYGNSS Algorithm Theoretical Basis Document. UM Doc. No. 148-0400, Rev 1, 3 Mar 2021.

[25] Mayers, D. R., C. S. Ruf, and A. M. Warnock, 2023: CYGNSS Storm-Centric Tropical Cyclone Gridded Wind Speed Product. *J. Appl. Meteor. Climatol.*, **62**, 329–339, https://doi.org/10.1175/JAMC-D-22-0054.1.

[26] CYGNSS. 2021. CYGNSS Level 3 Storm Centric Grid Science Data Record Version 1.0. Ver. 1.0. PO.DAAC, CA, USA. Dataset accessed [YYYY-MM-DD] at https://doi.org/10.5067/CYGNS-L3S10 .

[27] Ricciardulli, L.; Mears, C.; Manaster, A.; Meissner, T. Assessment of CYGNSS Wind Speed Retrievals in Tropical Cyclones. *Remote Sens.* **2021**, *13*, 5110. https://doi.org/10.3390/rs13245110

[28] CYGNSS. 2024. CYGNSS L3 MRG Science Data Record Version 3.2. Ver. 3.2. PO.DAAC, CA, USA. Dataset accessed [2024-02-22] at https://doi.org/10.5067/CYGNS-L3M32

[29] Landsea, C. W., and J. L. Franklin, 2013, "Atlantic Hurricane Database Uncertainty and Presentation of a New Database Format," Mon. Wea. Rev., 141, 3576–3592, https://doi.org/10.1175/MWR-D-12-00254.1.

[30] Joint Typhoon Warning Center, 2024a. "Western North Pacific Ocean Best Track Data," distributed by the Joint Typhoon Warning Center. https://www.metoc.navy.mil/jtwc/jtwc.html?western-pacific

[31] Joint Typhoon Warning Center, 2024b. "North Indian Ocean Best Track Data," distributed by the Joint Typhoon Warning Center. https://www.metoc.navy.mil/jtwc/jtwc.html?north-indian-ocean

[32] Joint Typhoon Warning Center, 2024c. "Southern Hemisphere Best Track Data," distributed by the Joint Typhoon Warning Center. https://www.metoc.navy.mil/jtwc/jtwc.html?southern-hemisphere

[33] Gopalakrishnan, Sundararaman, et al. "Hurricane Weather Research and Forecasting (HWRF) model: 2011 scientific documentation." *L. Bernardet, Ed* (2011).

[34] Meissner, T., L. Ricciardulli, and F. Wentz, 2018: Remote Sensing Systems SMAP daily Sea Surface Winds Speeds on 0.25 deg grid, Version 01.0. [NRT or FINAL]. Remote Sensing Systems, Santa Rosa, CA. Available online at www.remss.com/missions/smap/

[35] Balasubramaniam, R., and C. S. Ruf, 2023. Development and Application of a GNSS-R Error Model for Hurricane Winds. IEEE J. Selected Topics Appl. Earth Obs., 17, 2336-2346, https://doi.org/10.1109/JSTARS.2023.3344371.

April M. Warnock received the B.S.E. degree in earth systems & science engineering and the M.S.E. and Ph.D. in civil engineering from the University of Michigan, Ann Arbor, MI, USA in 2008, 2009, and 2013, respectively. She was a Post-Doctoral Research Associate with the Coastal Hydroscience Analysis, Modeling, and Predictive Simulations Laboratory at the University of Central Florida, Orlando, FL, USA. She is currently a Principal Research Engineer with SRI International, Ann Arbor, MI, USA. Her research interests include remote sensing, environmental hydrodynamics, inverse modeling, wave modeling, and riverine characterization.

Christopher S. Ruf (Life Fellow, IEEE) received the B.A. degree in physics from the Reed College, Portland, OR, USA, in 1982, and the Ph.D. degree in electrical and computer engineering from the University of Massachusetts at Amherst, Amherst, MA, USA, in 1987. He has worked at Intel Corporation, Aloha, OR, USA; Hughes Space and Communication, El Segundo, CA, USA; the National Aeronautics and Space Administration (NASA) Jet Propulsion Laboratory, Pasadena, CA, USA; and Pennsylvania State University, University Park, PA, USA. He is currently the Frederick Bartman Collegiate Professor of climate and space science and the Director of the Space Institute, University of Michigan, Ann Arbor, MI, USA, and a Principal Investigator of the NASA Cyclone Global Navigation Satellite System (CYGNSS) Mission. His research interests include remote sensing technology, methods, and applications. Prof. Ruf is a member of the American Geophysical Union (AGU) and the American Meteorological Society (AMS) and Vice-Chair of Commission F of the URSI. He is former Editor-in-Chief of the IEEE Transactions on Geoscience and Remote Sensing. He has served on the editorial boards of Radio Science, Journal of Atmospheric and Oceanic Technology, and Scientific Reports.

Mohammad M. Al-Khaldi (Member, IEEE) received the bachelor's degree in electrical engineering from the American University of Sharjah, Sharjah, United Arab Emirates, in 2015, the M.S. degree in electrical engineering from Texas A&M University, College Station, TX, USA, in 2017, the M.S. degree in electrical and computer engineering from The Ohio State University, Columbus, OH, USA, in 2019, and the Ph.D. degree from the Department of Electrical and Computer Engineering, and the ElectroScience Laboratory, The Ohio State University, in 2020.,He was a Project Scientist I, a Post-Doctoral Fellow II, and a Post-Doctoral Fellow I with the COSMIC Program, University Corporation for Atmospheric Research (UCAR), Boulder, CO, USA. He is currently a Senior Research Associate at the ElectroScience Laboratory and the Department of Electrical and Computer Engineering, The Ohio State University. He is also a member of the NASA Cyclone Global Navigation Satellite System (CYGNSS) Mission Science Team and the NASA CYGNSS Mission Calibration and Validation Team. His research interests include applied electromagnetics, rough surface scattering, and spaceborne remote sensing. Dr. Al-Khaldi is a member of the IEEE Geoscience and Remote Sensing Society (GRSS) Technical Committee on Modeling in Remote Sensing and the IEEE GRSS Technical Committees on Frequency Allocations in Remote Sensing. He is also an Associate Member of Commissions B and F of the International Union of Radio Science (URSI) and an NASA Commercial Smallsat Data Acquisition Program (CSDA) Global Navigation Satellite System Reflectometry (GNSS-R) Subject Matter Expert (SME), and serves as an Associate Editor for Radio Science.

Anthony Russel received the B.S. degree in computer science engineering from Michigan State University, East Lansing, MI, USA, in 2014. He is currently a member of the Engineering Staff at the Space Physics Research Laboratory, College of Engineering, University of Michigan, Ann Arbor, MI, USA. His primary engineering activities involve algorithm development and large-scale data processing as a member of the Science Operations Center for the Cyclone Global Navigation Satellite System (CYGNSS) mission.

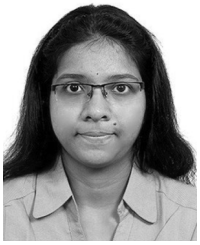

Rajeswari Balasubramaniam (Member, IEEE) received the B.E. degree in electrical and electronics engineering from Anna University, Chennai, India, in 2014, the M.E. degree in geoinformatics with a specialization in remote sensing and image processing from the Indian Institute of Space Science and Technology, Thiruvananthapuram, India, in 2016, and the Ph.D. degree from the Department of Climate and Space Sciences and Engineering, University of Michigan, Ann Arbor, MI, USA, in 2020. Her current work focuses on various aspects of calibration and validation for the NASA Cyclone Global Navigation Satellite System (GNSS) Mission. Her research interests include GNSS reflectometry, statistical signal processing, remote sensing inversion theory, data analysis, and microwave engineering.